Applied Catalysis B: Environmental 126 (2012) 134–143

Contents lists available at SciVerse ScienceDirect

Applied Catalysis B: Environmental

journal homepage: www.elsevier.com/locate/apcatb

Influence of lanthanum stoichiometry in $La_{1-x}FeO_{3-\delta}$ perovskites on their structure and catalytic performance in CH_4 total oxidation

Jérémy Faye[a,*], Alexandre Baylet[a], Martine Trentesaux[b], Sébastien Royer[a,c], Franck Dumeignil[b,d], Daniel Duprez[a,c], Sabine Valange[a,c], Jean-Michel Tatibouët[a,c]

[a] Laboratoire de Catalyse en Chimie Organique, CNRS UMR 6503, Université de Poitiers, 40 avenue du Recteur Pineau, F-86022 Poitiers Cedex, France
[b] Unité de Catalyse et Chimie du Solide, UMR CNRS 8181, Université Lille Nord de France, F-59655 Villeneuve d'Ascq Cedex, France
[c] Institut de Chimie des Milieux et Matériaux de Poitiers (IC2MP), CNRS UMR 7285, Université de Poitiers, Ecole Nationale Supérieure d'Ingénieurs de Poitiers, 1 rue Marcel Doré, F-86022, Poitiers Cedex, France
[d] Institut Universitaire de France, Maison des Universités, 103 Boulevard Saint-Michel, F-75005 Paris, France

ARTICLE INFO

Article history:
Received 29 February 2012
Received in revised form 5 July 2012
Accepted 16 July 2012
Available online 23 July 2012

Keywords:
CH_4 total oxidation
Non-stoichiometric perovskite
XPS
Redox properties
Iron oxide

ABSTRACT

A series of iron-based $La_{1-x}FeO_{3-\delta}$ perovskites (with $x = 0$, 0.1, 0.2, 0.3 and 0.4) was prepared by the so-called self-combustion method using glycine as an ignition promoter. The chemical, structural and surface properties of these mixed oxides were thoroughly characterized before the determination of their activity in the total oxidation of methane. The catalytic data indicated a strong dependence of the methane conversion towards the catalyst elemental composition. A progressive Fe_2O_3 enrichment of the perovskite surface was clearly evidenced by XPS characterization when decreasing the lanthanum content of the solid. Such additional undesirable surface iron oxide induced an inhibiting effect on the catalytic activity. As a result, while the $La_{1-x}FeO_{3-\delta}$ ($x = 0$, 0.1, 0.2, 0.3, 0.4) perovskites presented moderated performances in methane total oxidation, the most efficient lanthanum iron-based perovskite is the stoichiometric $LaFeO_3$ mixed-oxide that exhibits the most adapted surface and global composition, resulting in a CH_4 conversion of 86% at 873 K.

1. Introduction

Regarding the disastrous greenhouse effect mainly attributed to volatile organic compounds (VOCs) and hydrocarbons, environmental legislations strongly encourage the development of new or enhanced processes for curbing the atmospheric pollution. In this respect, the catalytic oxidation of hydrocarbons, and more particularly methane, was largely reported in the literature over a wide variety of solids [1–3]. This reaction is conventionally performed over supported noble metals [2,4–6]. However, despite their high activity, noble metal-based formulations remain expensive and suffer from deactivation at intermediate temperatures (typically between 773 and 873 K) [6,7]. This deactivation phenomenon was clearly evidenced over palladium supported catalysts, to which the reduction with time on stream of the active PdO_x species to less active metallic palladium species (Pd^0) was accompanied by a progressive decrease in the methane conversion [8,9]. With the aim of avoiding the use of such expensive catalysts, intensive researches focused on the preparation of transition metal-based catalysts. Oxidic perovskites, which are among the most largely studied oxides over the last 35 years, exhibit high activities in oxidation reactions [10–15]. While perovskites authorize numerous formulation variations (the perovskite structure being achieved if the tolerance factor defined as a function of the ionic radii of the cations and the oxygen ion, $t = (r_{Ln} + r_O)/\sqrt{2}(r_B + r_O)$, is comprised between 0.8 and 1, while respecting the electroneutrality in the structure), only a few number of compositions and especially $LnBO_3$ solids (with Ln being a lanthanide and B a transition metal) are efficient in oxidation reactions. In some rare cases, mixed-oxide catalysts even exhibited activities comparable to that of reference supported noble-metal catalysts. For example, Arai et al. [16] reported similar activities over $La_{1-x}Sr_xMnO_3$ and a reference 1% Pt/Al_2O_3 for the CH_4 total oxidation reaction. A recent work in our laboratory also evidenced that perovskites could compete with noble metal-doped mixed-oxides in terms of catalytic activity, especially for the oxidation of refractory hydrocarbons such as CH_4 [8]. Pioneering works [10–14] inspired many academic studies on the properties of such solids related to a variety of hydrocarbons oxidation reactions. Perovskites were even successfully incorporated in three-ways catalyst formulations by Daihatsu Motors [17]. It was generally reported that, among the possible compositions, cobalt and manganese-based solids exhibited the highest activities while

* Corresponding author at: Unité de Catalyse et Chimie du Solide, UMR CNRS 8181, Université Lille Nord de France, F-59655 Villeneuve d'Ascq Cedex, France.
Tel.: +33 0 3 20 33 64 38; fax: +33 0 3 20 43 65 61.
E-mail address: jeremy.faye@univ-lille1.fr (J. Faye).

0926-3373/$ – see front matter © 2012 Elsevier B.V. All rights reserved.
http://dx.doi.org/10.1016/j.apcatb.2012.07.001

lower performances were generally reported with nickel or iron in B position in the structure [18–20]. Most of the studies on perovskites are based on lanthanum placed in A-position. However, the effect of the A-cation – as a general matter chosen among the rare-earth elements – on the catalytic activity remains unclear [19,21–23]. The oxidation mechanisms over these catalysts are rather complex. In 1976, Voorhoeve et al. [24] introduced the concepts of suprafacial and interfacial mechanisms in order to explain the differences in behavior of the perovskites at low and high oxidation reaction temperatures. The suprafacial mechanism implies a reaction between adsorbed oxygen species on the catalyst surface (typically O^-), while interfacial reaction occurs between adsorbed reactants and lattice oxygen (O^{2-}) at temperatures enabling its activation. A good example of interfacial reaction was given by Arai et al. [16] for methane combustion: the fully oxidized transition metal (Co^{3+}, Mn^{4+}, Fe^{3+}, Cu^{2+}, Ni^{3+}, Cr^{4+}) was firstly partially reduced (into Co^{2+}, Mn^{3+}, Fe^{2+}, Cu^{+}, Ni^{2+}, Cr^{3+}) through consumption of lattice oxygen during total oxidation of methane, leading to the formation of anionic vacancies (Eq. (1)). Then, the vacancies were replenished with lattice oxygen driven from the bulk to the surface or using molecular oxygen from the gas phase, incorporated in the perovskite network (Eq. (2)). Thus, the transition metal returned to its initial oxidation state and was made available for further oxidation of the substrate (*e.g.*, CH_4).

$$M^{n+}\text{–}O^{a-} + CH_4 \rightarrow 4\,M^{(n-a)+}\text{–}\square + CO_2 + 2\,H_2O \quad (1)$$

$$4\,M^{(n-a)+}\text{–}\square + 2\,O_2 \rightarrow 4\,M^{n+}\text{–}O^{a-} \quad (2)$$

where M refers to the transition metal at the *n* oxidation state, O^{a-} to a surface active oxygen species with $a = 1$ or 2 and □ represents an anionic vacancy.

The oxygen mobility in the structure and the redox properties of the transition metal are thus crucial parameters that modulate the activity of perovskites in oxidation reactions [25]. These properties are strongly affected by the introduction of elements of different valencies such as Sr^{2+} or Ce^{4+} in the ABO_3 structure. Indeed, it is suggested that such substitutions promote the formation of either anionic or cationic vacancies, depending on the valency of the doping element [26–32]. Consequently, significant modifications of the transition metal reducibility and thereby of the catalytic activity were observed. A typical example was described by Nitadori et al. [29] over a series of $La_{1-x}Sr_xMnO_3$ perovskites. They reported a parallel evolution between the transition metal reducibility, the amount of labile oxygen, the rate of oxygen equilibration and the rate of propane oxidation.

The main objective of this work was to design a heterogeneous catalytic system for the total oxidation of methane and to highlight the role of the oxygen mobility/cation reducibility on the catalytic activity. The approach proposed in this work for enhancing the oxygen mobility differs from that generally found in the literature (*i.e.*, the substitution of the A- and/or B-cation by a heteroelement). Our strategy namely consisted in adjusting the redox properties of the perovskite by varying the stoichiometry of the A element. More precisely, iron was used as B-element in the perovskite and the atomic concentration of lanthanum was modulated, leading to solids having $La_{1-x}FeO_{3-\delta}$ as a general formula (with $x = 0$, 0.1, 0.2, 0.3 and 0.4). XPS analysis enabled determination of the catalysts surface composition, while the iron redox properties were evaluated by temperature programmed reduction under H_2. The solids were further tested for the total oxidation of methane. The catalytic performance of the whole $La_{1-x}FeO_{3-\delta}$ series was correlated with their bulk and surface properties.

2. Experimental

2.1. Catalysts synthesis

$La_{1-x}FeO_{3-\delta}$ mixed-oxides were prepared by the self-combustion method already successfully used in our laboratory for the synthesis of a large variety of mixed-oxides [33–35]. The amount of iron and lanthanum precursors was adjusted to obtain *ca.* 2.0 g of perovskite after the synthesis and calcination steps. The desired amount of nitrate precursors ($La(NO_3)_3{\cdot}6H_2O$ Rhodia 99.99%, $Fe(NO_3)_3{\cdot}9H_2O$ Prolabo 98%)), according to the nominal formula $La_{1-x}FeO_{3-\delta}$ with $x = 0$, 0.1, 0.2, 0.3 and 0.4, was first dissolved in water (10 mL). Then, glycine (NH_2–CH_2–COOH, Merck, pure) was slowly added to the solution so as to yield a molar ratio NO_3^-/NH_2 of 1. The resulting solution was heated at 373 K on a hot plate for 1 h under atmospheric conditions in order to evaporate the excess of water and further heated to 573 K until the auto-ignition process started (no heating rate control).

The presence of glycine enabled the ignition of the reactant mixture in moderate conditions (~573 K), while inducing a temperature increase by exothermicity which was sufficient to favor the crystallization of the perovskite. After grinding of the so-obtained orange powdery product, the sample was calcined for 8 h in a tubular quartz reactor at 873 K (heating rate = 5 K min^{-1}) under a 2 L min^{-1} dry air flow in order to eliminate the remaining carbonaceous residues coming from incomplete glycine combustion. This temperature is however too low to remove stable carbonate species known to form on the surface of such lanthanide-containing perovskite solids.

2.2. Characterization

The phase identification was carried out by X-ray diffraction at room temperature using a Siemens D5000 instrument (Cu $K_{\alpha1}$ = 1.5406 Å and Cu $K_{\alpha2}$ = 1.5439 Å, operating at 40 kV and 30 mA). X-ray diffractograms were recorded in the 2θ values range 20–80° with a rate of 0.04° and a step size of 2 s. *In situ* XRD experiments were performed on a Brücker D8Advance diffractometer with monochromatized Cu $K_{\alpha1}$ radiation. In this *in situ* procedure, the samples were deposited on a kanthal sample holder and XRD patterns were collected every 100 K from room temperature to 1273 K, under a gas mixture composed of 3% H_2 diluted in He (50 mL min^{-1}). All diffractograms were collected after 30 min after stabilizing the sample at the desired temperature. After the last temperature recording, sample was cooled down to 303 K for a last diffractogram recording. The phase identification was achieved by comparison with JCPDS files. *In situ* experiments allowed us to follow the evolution of the sample structure with the reduction degree. The mean crystal domain sizes (d_{LaFeO_3} and $d_{Fe_2O_3}$, Table 1) were determined by Rietveld refinement of the XRD pattern using the Fullprof Suite and its WinPLOTR interface [36].

The BET surface areas were determined by adsorption–desorption of nitrogen on a Micromeritics Tristar apparatus. After introducing about 0.5 g of powder in the analysis cell, the sample was first outgassed at 523 K for 6 h. After cooling to room temperature, the cell was backfilled with helium and transferred to the analysis port of the instrument. The cell containing the sample was then immersed in a Dewar filled with liquid nitrogen and exposed to pure N_2 at partial pressures P/P_0 between 0.01 and 0.2 (5 points). The specific surface area (SSA, Table 1) of each sample was deduced from the linear part of the BET plots $P/P_0 = 1/\upsilon[(P_0/P) - 1]$, where P and P_0 are the equilibrium and the saturation pressure of N_2 at 77 K, respectively, and υ is the adsorbed gas quantity.

The H_2-Temperature Programmed Reduction experiments (H_2-TPR) were performed on a Micromeritics AutoChem 2910

Table 1
Physical and crystalline properties of the $La_{1-x}FeO_{3-\delta}$ samples.

Sample name	Stoichiometry[a]	Crystalline phases[b]	d_{LaFeO_3}[c] (nm)	$d_{Fe_2O_3}$[c] (nm)	SSA[d] ($m^2\,g^{-1}$)
LaFe	$La_{0.94}FeO_{3-\delta}$	$LaFeO_3$	26	–	20
$La_{0.9}Fe$	$La_{0.83}FeO_{3-\delta}$	$LaFeO_3$	21	–	23
$La_{0.8}Fe$	$La_{0.76}FeO_{3-\delta}$	$LaFeO_3/Fe_2O_3$	20	–	20
$La_{0.7}Fe$	$La_{0.64}FeO_{3-\delta}$	$LaFeO_3/Fe_2O_3$	26	23	23
$La_{0.6}Fe$	$La_{0.55}FeO_{3-\delta}$	$LaFeO_3/Fe_2O_3$	20	20	18

[a] Stoichiometry evaluated by ICP after dissolution of the samples in a concentrated HCl/HNO_3 mixture.
[b] Crystalline phases identified by X-ray diffraction.
[c] Perovskite/Fe_2O_3 crystal domain sizes evaluated by Rietveld refinement of X-ray patterns (see Section 2).
[d] Specific surface area obtained from the BET equation.

instrument. After a first outgassing treatment under Ar (flow rate = 50 mL min^{-1}) up to 723 K (heating rate = 10 K min^{-1}) for 10 min, the sample (50 mg) was treated under vacuum and then cooled to room temperature. After stabilization of the reducing flow (H_2:Ar = 5:95 [vol.%], total flow rate = 50 mL min^{-1}), the temperature was increased from room temperature to 1273 K (heating rate of 10 K min^{-1}) and kept at this temperature during 150 min so that to achieve the total reduction of the solids. Hydrogen consumption was recorded using TCD detection.

X-ray Photoelectron Spectroscopy (XPS) experiments were carried out on a VG Escalab 220XL spectrometer running under ultrahigh vacuum (UHV at *ca.* 10^{-10} Torr). X-rays of 1486.6 eV were produced by an aluminum anode (15 kV, 20 mA). High resolution spectra were collected in the constant analysis energy mode (CAE = 40 eV). All the binding energies were calibrated with the C1s binding energy fixed at 285 eV as an internal reference. The surface atomic ratios were calculated by correcting the intensity with theoretical sensitivity factors based on the Scofield cross-sections. The curve fittings were achieved with the CasaXPS software using the following binding energies regions for the quantitative analyses: C1s, O1s, Fe2p and La3d.

2.3. Total oxidation of methane

The catalytic activity of the $La_{1-x}FeO_{3-\delta}$ solids was evaluated in the total oxidation of methane reaction (Eq. (3)):

$$CH_4 + 2\,O_2 \rightarrow CO_2 + 2\,H_2O \quad (3)$$

50 mg of catalyst were diluted in 250 mg of carborundum and introduced in a U-shaped quartz reactor (I.D. = 5 mm) between two quartz wool plugs. The catalysts were activated under air at 873 K for 1 h (heating rate of 10 K min^{-1}, total flow rate of 200 cm^3 min^{-1}), before being cooled to room temperature under the same flow prior to reaction. After purging the reactor under N_2 at 323 K, the reactant mixture composed of $CH_4/O_2/N_2$ = 0.5/19.5/80 (vol.%) was passed through the catalytic bed at a total flow rate of 190 mL min^{-1}, yielding a GHSV of 240,000 mL g^{-1} h^{-1}. After stabilization of the reactant mixture composition at the outlet of the reactor, the catalytic bed temperature was increased to 873 K at a rate of 5 K min^{-1}. The light-off curves presented in this study correspond to the methane conversion determined by sampling every 75 s. The gas phase composition was determined using a Varian GC3900 chromatograph equipped with a Porapak Q packed column (I.D. = 6 mm, L = 0.3 m) connected to a flame ionization detector (FID).

The methane conversion, X_{CH_4}, was calculated according to the following equation:

$$X_{CH_4} = \frac{x^0_{CH_4} - x^T_{CH_4}}{x^0_{CH_4}} \times 100 \quad (4)$$

where $x^0_{CH_4}$ refers to the volumetric concentration of methane in the feed and $x^T_{CH_4}$ corresponds to the concentration of methane at the operating T temperature.

3. Results and discussion

3.1. Chemical composition and texture of the perovskites

The chemical composition of the samples determined by ICP is given in Table 1. For all samples, the experimental composition remained close to the nominal one (within a 10% error), which allowed us to reliably study the influence of the A cation stoichiometry on the structure, redox and catalytic properties. This error above-mentioned can be related to incertitude in metals precursor hydration degrees and led to elemental compositions slightly different from the ones expected.

Irrespective of the A element loading, the specific surface areas (Table 1) of the samples exhibited a mean value of $20 \pm 3\,m^2\,g^{-1}$. In contrast with the results reported by Delmastro et al. [37] and Spinicci et al. [38] who prepared a series of $La_{1-\square}FeO_{3-1.5\square}$ using glycerol as fuel, no significant increase in surface area could be observed with the decrease in the lanthanum content. The SSA values obtained in this work are in the same range of order than those reported for perovskite samples calcined at similar temperatures. Indeed, the most widespread synthesis used to prepare perovskite materials, *i.e.*, the citrate complexation procedure, enables the preparation of lanthanum-based perovskites exhibiting surface areas that rarely exceed $20\,m^2\,g^{-1}$, irrespective of the transition metal in B-position in the crystal. For example, Pecchi et al. [39] reported surface area values ranging from 5 to 21 $m^2\,g^{-1}$ for a series of $LaFe_{1-x}Ni_xO_3$ solids calcined at 973 K. Even using higher calcination temperatures (1073 K), Ciambelli et al. [40] found surface areas of $5.0 \pm 1.0\,m^2\,g^{-1}$ for $LaFe_{1-x}Al_xO_3$ solids. The SSA values mentioned in the present work using the self-combustion procedure are also in agreement with those reported for solids prepared following such a synthesis route. The SSA of perovskite-type oxides

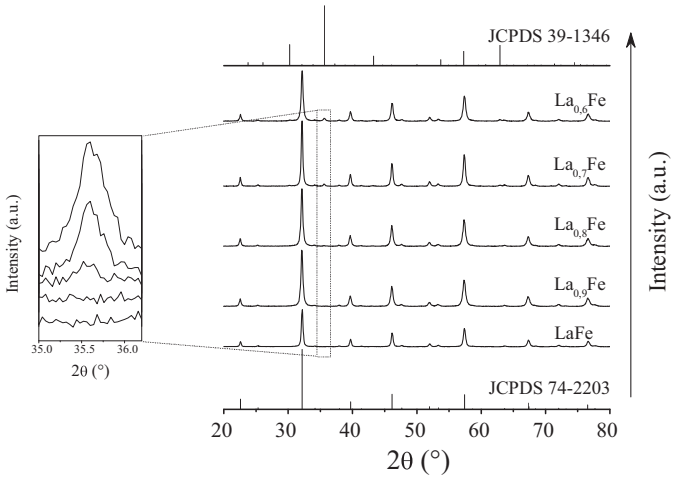

Fig. 1. X-ray diffractrograms of the calcined $La_{1-x}FeO_{3-\delta}$ samples. Ref: JCPDS 74-2203, $LaFeO_3$; JCPDS 39-1346, Hematite α-Fe_2O_3.

Table 2
Binding energies and relative surface abundances of the elements constituting the $La_{1-x}FeO_{3-\delta}$ samples.

Sample name	Fe/La atomic ratio		C1s		O1s		$La3d_{5/2}$		$Fe2p_{3/2}$	
	ICP	XPS	BE (eV)	at.%	BE (eV)	at.%	BE (eV)	at.%	BE (eV)	at.%
LaFe	1.06	0.42	285	13.0	529.1	55.2	833.8	22.4	710.1	9.4
$La_{0.9}Fe$	1.20	0.71	285	16.3	529.5	51.1	833.9	19.1	710.4	13.5
$La_{0.8}Fe$	1.32	0.96	285	23.2	529.3	50.8	833.8	13.3	710.5	12.7
$La_{0.7}Fe$	1.56	1.19	285	15.3	529.5	50.8	834.1	15.5	710.6	18.4
$La_{0.6}Fe$	1.82	1.24	285	25.1	529.7	48.0	834.0	12.0	710.6	14.9

was generally shown to vary up to 20 $m^2\ g^{-1}$ (~8 $m^2\ g^{-1}$ for $LaFeO_3$ [41]) even if some authors reported higher surface area values (up to 45 $m^2\ g^{-1}$ [42]).

3.2. Crystalline structure

The X-ray diffractograms of the $La_{1-x}FeO_{3-\delta}$ mixed oxides are presented in Fig. 1 as well as the stick diagrams summarizing information of the reference $LaFeO_3$ and α-Fe_2O_3 JCPDS files. The main structural properties of the $La_{1-x}FeO_{3-\delta}$ series are gathered in Table 1.

X-ray diffraction patterns of the whole calcined $La_{1-x}FeO_{3-\delta}$ series exhibited intense reflections readily attributed to the orthorhombic $LaFeO_3$ phase (JCPDS file n° 74-2203). This clearly confirmed that the calcination temperature used in this work, *i.e.*, 873 K, was sufficient to crystallize the precursor into the perovskite structure, even at the lowest lanthanum stoichiometry ($La_{0.6}Fe$ sample). This result is in agreement with literature data since it has been largely reported that the self-combustion synthesis route lead to the crystallization of an almost pure phase, as deduced from XRD analysis. For example, we previously successfully synthesized $LaBO_3$ (with B = Fe, Co and Ni) [43,44] and La_2NiO_4 [35] mixed-oxides using similar experimental conditions. This synthesis procedure is widely used for the preparation of perovskites, since it can lead to the crystallization of oxides exhibiting a relatively high SSA (of *ca.* 20 $m^2\ g^{-1}$), by limiting the crystal domain size [39,45]. In fact, a high reaction temperature during a very short time is achieved during the synthesis step, thereby preventing the sintering of the solid particles. Moreover, numerous references dealing with the crystallization of perovskites by the self-combustion route using different fuels such as glycine ($LaAlO_3$ [46]; $LaFeO_3$ [41]), ammonia ($BaZrO_3$ [47]) or urea ($La_{1-x}Sr_xO_3$ [42]) can be found. In all cases, the authors reported a pure crystalline structure as determined by XRD.

Besides the previously mentioned $LaFeO_3$ detected peaks, the diffractograms obtained for the samples having lanthanum stoichiometry lower than 0.8 ($La_{0.8}Fe$, $La_{0.7}Fe$ and $La_{0.6}Fe$; Table 1) exhibited additional diffraction lines corresponding to the hematite α-Fe_2O_3 variety (JCPDS file n° 39-1346; Fig. 1). A clear increase in the intensity of the main peak at $2\theta \approx 36°$ was observed with the decrease in lanthanum stoichiometry. This suggests that the decrease in lanthanum content of the solids does not result in the formation of a non-stoichiometric $La_{1-x}\square_xFeO_{3-1.5x}$ structure, where $\square$ refers to cationic vacancies, but in the formation of stoichiometric perovskite $LaFeO_3$ together with Fe_2O_3.

The crystal domain size of the perovskite phase was refined by Rietveld method and is observed to vary from 20 nm ($La_{0.8}Fe$; Table 1) to 26 nm (LaFe and $La_{0.7}Fe$; Table 1). Due to the signal/noise ratio of the diffraction lines for the $La_{0.8}Fe$ sample, it was not possible to evaluate a reliable mean particle size of the additional Fe_2O_3 phase. However, the refinement of the XRD patterns of $La_{0.7}Fe$ and $La_{0.6}Fe$ indicated a crystallite size of 23 and 20 nm respectively. Therefore, it could be concluded that both the perovskite and iron oxide crystal domain sizes were not strongly affected by the decrease in the lanthanum content, since the value remained always centered at 23 ± 3 nm. The crystal domain size values were in accordance with those reported in the literature over perovskite samples treated at similar calcination temperature. Indeed, crystal domain sizes ranging from 20 to 30 nm are widely reported in the literature for perovskite samples after calcination at 873 K [42,48,49].

3.3. Surface analysis

The nature and relative abundances of the surface species were determined by X-ray photoelectron spectroscopy (XPS). Table 2 summarizes the binding energies (BEs) of the C1s, O1s, $Fe2p_{3/2}$, $La3d_{5/2}$ levels as well as the calculated relative abundances.

First, the Fe/La surface ratio determined by XPS analysis was significantly lower than the bulk one determined by ICP (Table 2). In other words, these results suggested enrichment in lanthanum on the surface of the oxides. While a Fe/La ratio of 1.06 was expected for the LaFe sample, the XPS quantification led to a value of only 0.42. This is consistent with the literature that often reports surface lanthanum enrichment for La-based perovskites. For example, Barbero et al. reported a Fe/La ratio of 0.45 over $LaFeO_3$ synthesized by citrate complexation procedure followed by calcination at 973 K [50]. Moreover, a lanthanum bulk stoichiometry of 0.8 ($La_{0.8}Fe$ sample) was necessary to obtain a Fe/La ratio close to the unit (Table 2). At lower lanthanum stoichiometry, the surface of the solid presented an enrichment in iron (Fe/La ratio larger than 1), which increased with the decrease in lanthanum content ($La_{0.7}Fe$

Table 3
Atomic distribution in carbon and oxygen containing surface species obtained from the O1s and C1s spectral fitting.

Sample name	O1s spectral decomposition (at.%)[a]				C1s spectral decomposition (at.%)[b]	
	O_{LaFeO_3}	$O_{Fe_2O_3}$	$O_{CO_3^{2-}}$	O_{O_2}	$C_{CO_3^{2-}}$	$C_{amorphous}$
LaFe	34.5	1.4	14.8 (15.0)[c]	4.5	5.0	8.0
$La_{0.9}Fe$	16.4	19.4	13.0 (13.8)	2.3	4.6	11.7
$La_{0.8}Fe$	25.6	10.9	11.6 (11.7)	2.7	3.9	19.3
$La_{0.7}Fe$	12.6	24.6	10.5 (9.9)	3.1	3.3	12.0
$La_{0.6}Fe$	12.6	23.8	9.3 (9.3)	2.3	3.1	22.0

[a] The O1s spectral decomposition was performed considering four contributions: O_{LaFeO_3} (529.1 eV), $O_{Fe_2O_3}$ (529.7 eV), $O_{CO_3^{2-}}$ (531.7 eV) and O_{O_2} (527.7 eV).

[b] The C1s spectral decomposition was performed considering the two following contributions: $C_{CO_3^{2-}}$ (289.1 eV) and $C_{amorphous}$ (285.0 eV).

[c] Values indicated in parentheses (column 4) were calculated as follows: $O_{CO_3^{2-}} = 3 \times C_{CO_3^{2-}}$.

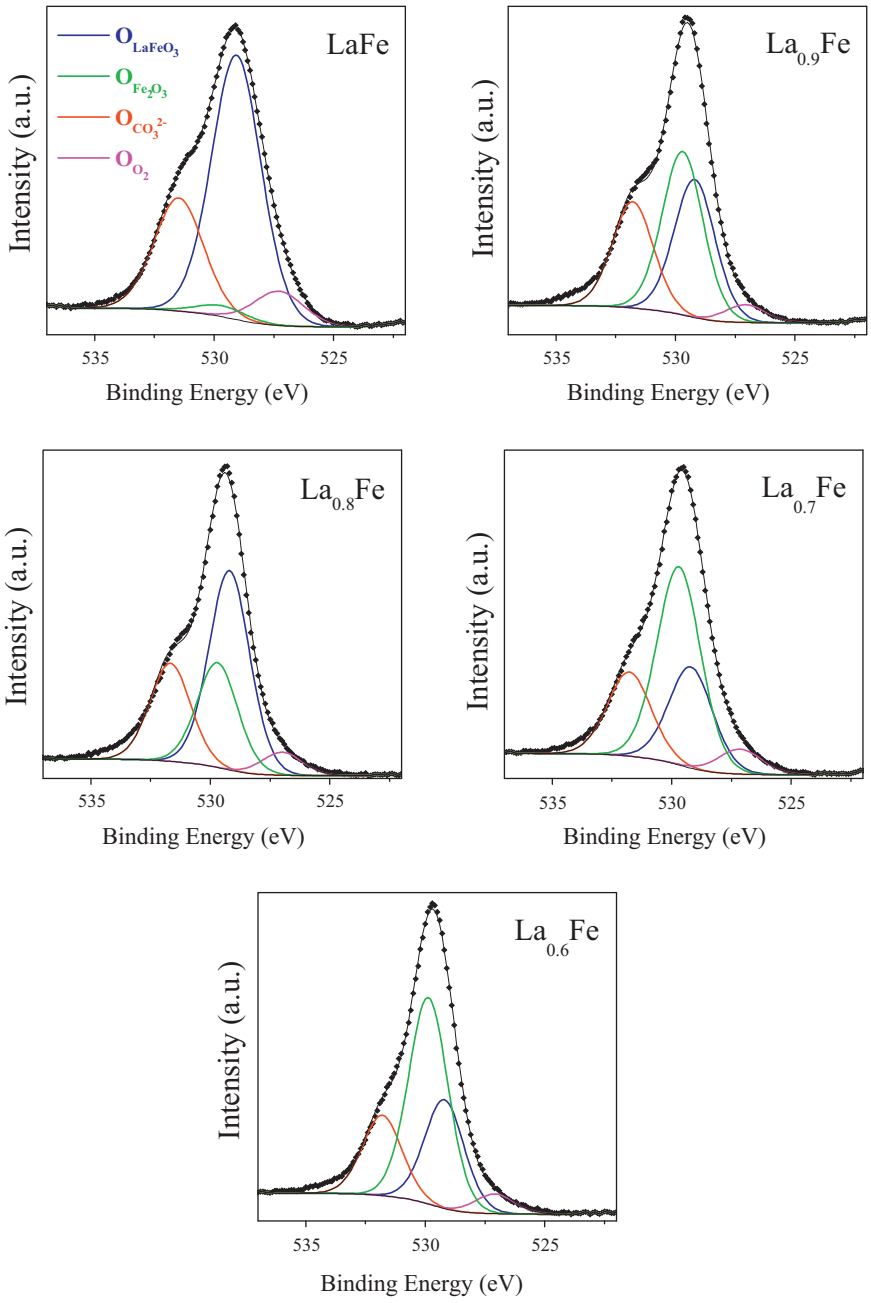

Fig. 2. Spectral decomposition of the O1s core level spectra obtained for the $La_{1-x}FeO_{3-\delta}$ series.

and $La_{0.6}Fe$, Table 2). Nevertheless, in any case, the Fe/La surface ratio remained lower than the nominal one.

Detailed information on the distribution of surface oxidized species was obtained by the careful analysis of the O1s spectra. The obtained O1s curve fittings are presented in Fig. 2 and the deduced atomic surface concentrations are summarized in Table 3.

The O1s envelops appeared at a glance as being composed of a main peak located at *ca.* 529.4 eV with a shoulder at *ca.* 531.7 eV. However, variations in the binding energy at the maximum intensity of the O1s peak were observed. Direct comparison of the LaFe O1s spectrum with that of $La_{0.6}Fe$ revealed a shift toward higher binding energies from 529.1 eV for the LaFe sample to 529.7 eV for the $La_{0.6}Fe$ sample. This suggests the contribution of more than 2 species to the O1s peaks global shape. This observation was consistent with XPS spectra reported in the literature for similar solids [51,52] for which various species were observed, such as lattice oxygen, but also adsorbed species like hydroxyl anions (dissociated water), carbonates or surface oxygen [53,54]. Therefore, the collected O1s envelops were fitted by taking into account the four following contributions:

1. Adsorbed molecular oxygen, at ~527.2 eV [54]
2. O^{2-} in $LaFeO_3$, at ~529.1 eV [39]
3. O^{2-} in Fe_2O_3, at ~529.7 eV [55]
4. O^* in CO_3^{2-}, at ~531.7 eV [39]

First of all, fitting enabled to ascribe the aforementioned peak shift toward the higher binding energies to a progressive enrichment in iron oxide on the surface. Indeed, the amount of oxygen attributed to Fe_2O_3 increased from 1.4 at.% to 23.8 at.% between the LaFe and $La_{0.6}Fe$ samples. This result showed that the

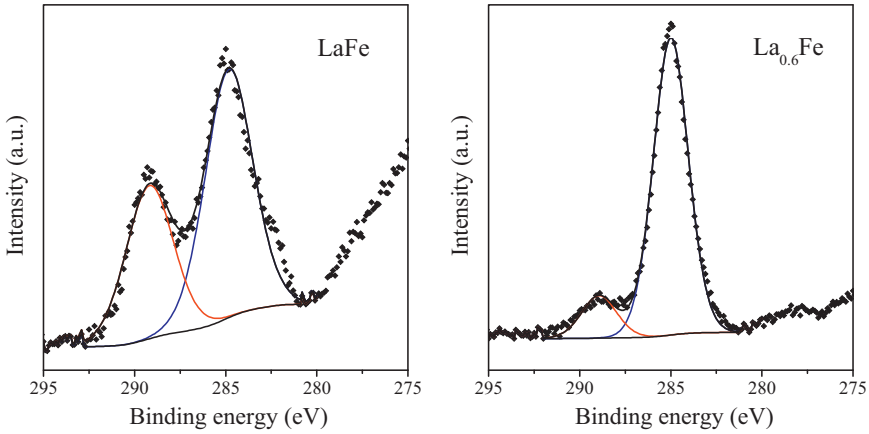

Fig. 3. Typical C1s core level spectra obtained for the $La_{1-x}FeO_{3-\delta}$ series; cases of LaFe and $La_{0.6}Fe$.

surface enrichment in iron on the surface (Fe/La ratio; Table 2) was correlated with the appearance of Fe_2O_3 on the surface.

As a consequence, the proportion of oxygen in $LaFeO_3$ (BE = 529.1 eV) decreased from 34.5 at.% for LaFe to 12.6 at.% for $La_{0.6}Fe$. In addition to the oxygen contributions corresponding to lattice O^{2-} in Fe_2O_3 and $LaFeO_3$, the curve fitting also evidenced variations in the proportion of oxygen species located at 531.7 eV, associated with the presence of carbonates on the surface [39]. The quantity of these latter decreased with the decrease in lanthanum stoichiometry (Fig. 2 and Table 3) from 14.8 at.% for LaFe to 9.3 at.% for $La_{0.6}Fe$. Thus, it was reasonable to correlate this evolution with the XPS analysis of carbon to complete the surface investigations. In contrast with the results obtained from surface oxygen abundances that remained almost constant and close to 50 at.% for all the studied samples, the total carbon surface concentration varied between 13.0 and 25.1 at.% (Table 2). The analysis of the C1s core level spectra obtained for the different samples evidenced a second contribution at 289.1 ± 0.2 eV, in addition to the amorphous carbon contamination component located at 285 eV (Fig. 3 and Table 3). This former contribution was ascribed to the carbon in surface carbonate species [38,52,55].

Thermally stable surface carbonates are indeed easily formed by reaction between surface lanthanum and CO_2 from air [56]. These species showed stability at high pre-treatment temperature (up to 873–973 K) and were thus expected to be preserved under the ultra-high vacuum conditions of the XPS analysis. The curve fitting of the C1s signal led to the atomic quantification of the fraction of carbon in CO_3^{2-} species that varied from 5.0 at.% (LaFe, Table 3) and 3.1 at.% ($La_{0.6}Fe$, Table 3). A linear evolution of the concentration of carbon in surface carbonate species with the experimental surface Fe/La atomic ratio was observed (Fig. 4). This result is in agreement with the academic literature [53] and reflects the basic character of perovskites, mainly related to the rare earth element concentration at their surface.

Considering the presence of carbonate species under the CO_3^{2-} form and thus assuming an atomic ratio of 3 between oxygen and carbon for these species, it was possible to determine the atomic fraction of oxygen species involved in carbonates composition from the atomic fraction of C in CO_3^{2-} deduced from XPS analysis. The obtained values are indicated in parentheses in the $O_{CO_3^{2-}}$ column of Table 3. A remarkable correlation with the values determined from the direct O1s peak fitting was obtained. This definitely confirms that the contribution fixed at 531.7 eV was essentially related to oxygen in surface carbonate species. Finally, the contribution of the oxygen associated to molecular adsorbed species remained limited and almost stable for the $La_{1-x}FeO_{3-\delta}$ series (always lower than 4.5 at.%, Table 3). Surface evolutions were also observed when analyzing the Fe2p XPS spectrum (Fig. 5A). This latter appeared as a set of two peaks having a spin-orbit splitting value of 13.4 eV corresponding to the $Fe2p_{3/2}$ (710.1 eV) and $Fe2p_{1/2}$ (723.4 eV) core levels. Each peak presented a shake-up satellite located at a binding energy 8.1 eV higher, which is characteristic of Fe^{3+} species [57,58]. The Fe2p spectra comparison enabled the confirmation of surface enrichment in Fe_2O_3 by the progressive shift of the $Fe2p_{3/2}$ peak toward higher binding energies from 710.1 eV for the LaFe sample to 710.6 eV for $La_{0.6}Fe$. The obtained results were in agreement with $Fe2p_{3/2}$ binding energies reported in the literature [39,59] for Fe^{3+} in $LaFeO_3$ (710.3 eV) and values determined for $Fe2p_{3/2}$ above 710.8 eV in Fe_2O_3 [55]. It could then be concluded that the surface of the samples remained exclusively composed of trivalent iron (in perovskite or in iron oxide), irrespective of the lanthanum stoichiometry.

Finally, the XPS analysis of the $La_{1-x}FeO_{3-\delta}$ samples was completed with that of the La3d core-level spectra, which is illustrated in Fig. 5B for the LaFe sample. Two pairs of peaks located at 833.8 and 850.5 eV and a broader peak centered at 863.6 eV were observed and attributed to the $La3d_{5/2}$ and $La3d_{3/2}$ energy levels, respectively. Each peak presented a satellite at 3.8 eV higher, which is consistent with academic references on lanthanum containing oxides [57,59]. The broad satellite peak located at 863.6 eV

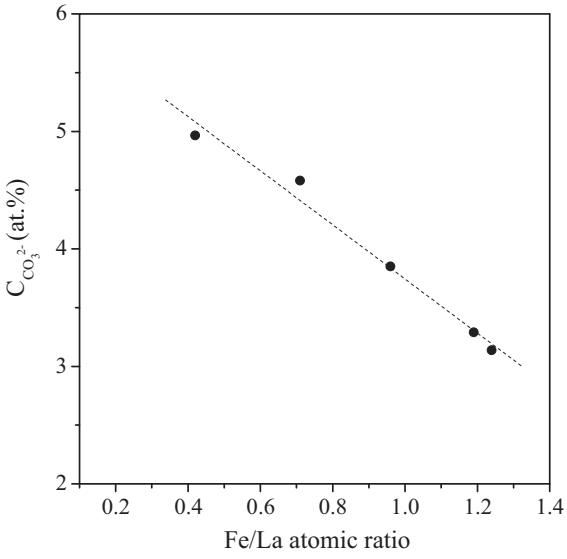

Fig. 4. Evolution of the surface carbonate species concentration as a function of the surface Fe/La atomic ratio.

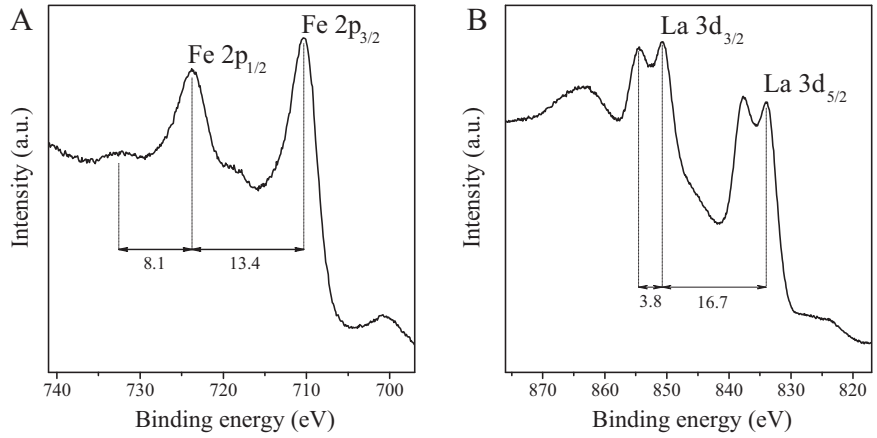

Fig. 5. Example of (A) Fe2p and (B) La3d core levels spectra obtained for the LaFe sample.

was ascribed to secondary electronic processes resulting from electronic interactions between lanthanum and oxygen [57]. The comparison between the La3d photolines for all the samples in the $La_{1-x}FeO_{3-\delta}$ series did not allowed us to evidence any change in the La $3d_{5/2}$ binding energy (833.9 ± 0.1 eV). However, when relating this result with the Fe/La ratio indicated in Table 2, the presence of one or more La-containing species on the surface is strongly suggested. Indeed, lanthanum segregation was observed for the LaFe and $La_{0.9}Fe$ samples with Fe/La ratio of 0.42 and 0.71 respectively. This suggests the presence of La-enriched species such as oxide, carbonate or oxycarbonate, in addition to the perovskite phase.

The detailed analysis of the XPS spectra confirmed the complexity in the distribution of the surface species of these mixed oxides depending on the elemental composition. All the results suggested that the surface exhibits a combination of $LaFeO_3$ perovskite and iron oxide. The relative distribution of these oxides followed that of the elemental composition: the lowest the lanthanum concentration, the highest the proportion of surface Fe_2O_3.

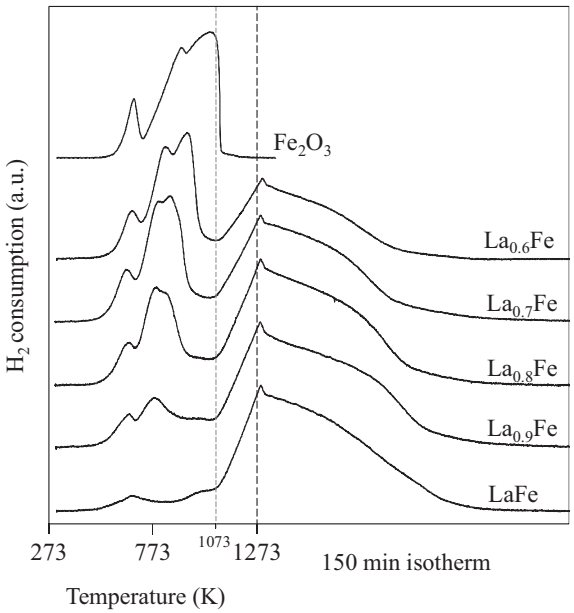

Fig. 6. Temperature programmed reduction profiles for the $La_{1-x}FeO_{3-\delta}$ samples.

3.4. Redox properties

Iron reducibility in the $La_{1-x}FeO_{3-\delta}$ series of samples was studied by temperature programmed reduction under hydrogen. The H_2-TPR reduction curves obtained for the different samples are presented in Fig. 6. The corresponding amounts of hydrogen consumed at the different steps of reduction (below and above 1073 K), as well as the respective amounts of Fe_2O_3 and $LaFeO_3$ calculated from the chemical analyses and by assuming that Fe is mainly contained in Fe_2O_3 and $LaFeO_3$ stoichiometric oxides, are summarized in Table 4.

Irrespective of the sample, the TPR profile proceeds in two steps corresponding to two temperature ranges, namely below and above 1073 K (Fig. 6). The hydrogen consumption peaks below 1073 K were globally centered at 773 K and increased in intensity with the decrease in lanthanum stoichiometry, while the intensity of the unique TPR peak for temperatures above 1073 K decreased at the same time.

To better understand the reduction mechanism, an *in situ* XRD experiment was conducted with the $La_{0.6}Fe$ sample to evidence the progressive Fe^{3+} reduction through the formation of intermediate phases. The diffractograms presented in Fig. 7 showed the progressive formation and reduction of the different crystalline phases as a function of temperature.

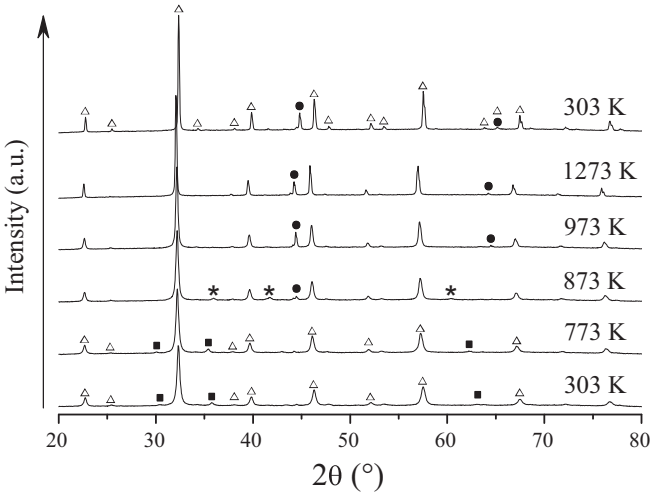

Fig. 7. *In situ* X-ray diffractograms of $La_{0.6}Fe$ during temperature programmed reduction. (△) $LaFeO_3$, (■) Fe_2O_3, (*) FeO, (●) Fe°.

Table 4
Parameters deduced from the H_2-TPR for the $La_{1-x}FeO_{3-\delta}$ oxides series.

Sample name	Experimental phase composition (mmol g^{-1})[a]			H_2 consumption (mmol g^{-1})		% Fe in Fe_2O_3 reduced to Fe^0[b]	% Fe totally reduced to Fe^0[c]
	$[Fe]_{LaFeO_3}$	$[Fe]_{Fe_2O_3}$	$[Fe]_{total}$	$T < 1073$ K	Total		
LaFe	4.04	0.24	4.28	0.52	6.37	142#	99
$La_{0.9}Fe$	3.85	0.80	4.65	1.12	6.55	94	94
$La_{0.8}Fe$	3.72	1.19	4.91	1.70	6.86	95	93
$La_{0.7}Fe$	3.47	1.96	5.43	2.46	7.33	84	90
$La_{0.6}Fe$	3.26	2.60	5.86	3.26	7.52	84	86

[a] Calculated amount of stoichiometric perovskite and Fe_2O_3 phase on the basis of ICP results.
[b] Percentage of Fe^{3+} in Fe_2O_3 phase reduced to Fe^0 (calculated on the basis of H_2 consumption below 1073 K).
[c] Percentage of Fe^{3+} reduced to Fe^0 at the end of H_2-TPR experiment (calculated on the basis of total H_2 consumption); # value above 100%, indicating the reduction of a fraction of iron in the perovskite.

The same crystal phases were observed up to 773 K, confirming that the $LaFeO_3$ structure remains the main component and that Fe_2O_3 is a secondary oxide. Structural modifications started at 873 K with a decrease in the intensities of the Fe_2O_3 reflections and the simultaneous formation of FeO (JCPDS file n° 89-2468) and Fe^0 (JCPDS file n° 87-0721). At 973 K, the ferrous oxide phase completely disappeared and only metallic iron remained visible by XRD, in addition to the signal of the initial perovskite structure. Increasing the temperature to 1273 K did not lead to any further modification of the diffraction patterns. However, the analysis of the diffraction patterns of the $La_{1-x}FeO_{3-\delta}$ series of samples obtained after H_2-TPR confirmed that the reduction process ended up with the formation of metallic iron and La_2O_3 in all cases, which is in accordance with the calculated values of total Fe^{3+} reduction to Fe^0 (Table 4). The incomplete perovskite reduction during the *in situ* XRD experiment (presence of both Fe^0 and $LaFeO_3$), although *a priori* surprising, can be easily rationalized if one considers the lower hydrogen concentration (3% H_2/He gas mixture) than that used for the H_2-TPR (5% H_2/Ar gas mixture), and the longer reduction time at 1273 K during the H_2-TPR process to ensure complete reduction of the catalyst (Fig. 6, isothermal region).

An H_2-TPR analysis of a pure iron oxide α-Fe_2O_3 (Fig. 6) prepared following the same self-combustion synthesis procedure was also carried out. As pointed out in many studies, the reduction of α-Fe_2O_3 is rather complex and can occur through multiple successive steps. In this study, a first step corresponding to the partial reduction of Fe^{3+} to Fe^{2+} with a hydrogen consumption peak located at 678 K was observed. The hydrogen consumption quantification at 715 K (end of the first peak) was about 10% and corresponded to an iron oxidation degree of +2.7. This value is in accordance with the formation of the Fe_3O_4 oxide phase (Eq. (4)). Thereafter, a shoulder was observed at 903 K, representative of the reduction of all the Fe^{3+} species into Fe^{2+} ones with an H_2 consumption extent of 40% ($Fe^{1.9+}$), leading to the possible formation of the FeO oxide phase (Equation 5). The presence of this phase has already been reported, *e.g.*, by Munteanu et al. [60], while other authors considered a one-step reduction of Fe_3O_4 to Fe^0 [61,62] (Eq. (6)). In our case, the presence of a highly pronounced shoulder in the Fe_2O_3 reduction profile strongly supports the formation of FeO as an intermediate phase. Finally, an intense hydrogen consumption peak was observed at 1033 K, corresponding to the reduction of the residual iron oxide species into Fe^0 (Eq. (7)).

$$Fe_2O_3 + H_2 \rightarrow 2\,Fe_3O_4 + H_2O \quad \text{(centered at 678 K)} \tag{4}$$

$$Fe_3O_4 + H_2 \rightarrow 3\,FeO + H_2O \quad \text{(centered at 903 K)} \tag{5}$$

$$Fe_3O_4 + 4H_2 \rightarrow 3\,Fe^0 + 4\,H_2O \tag{6}$$

$$FeO + H_2 \rightarrow Fe^0 + H_2O \quad (T > 1033\,K) \tag{7}$$

The TPR profile of the self-combustion Fe_2O_3 sample was compared with those of the $La_{1-x}FeO_{3-\delta}$ samples. In line with what was observed by *in situ* XRD (reduction of Fe_2O_3 to Fe^0 at 973 K), it was argued that the hydrogen consumption at the lowest TPR temperature should reflect the reduction of the Fe_2O_3 clusters to metallic Fe. To ascertain this hypothesis, the hydrogen consumption corresponding to the TPR peaks below 1073 K was determined and compared with the amount of Fe_2O_3 calculated from the chemical analysis (Table 4).

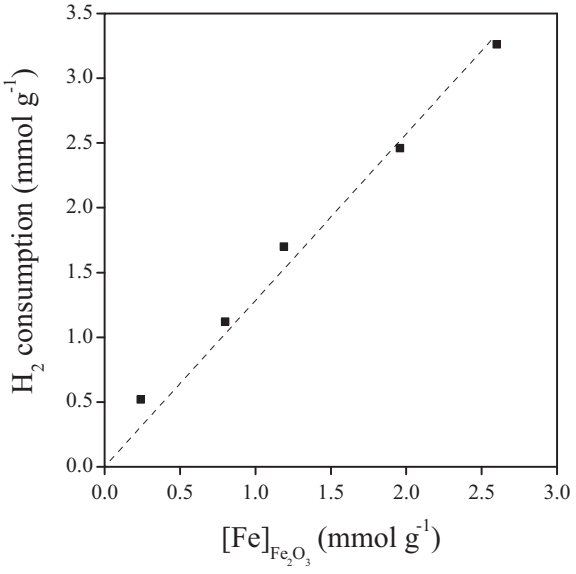

Fig. 8. Correlation between hydrogen consumption and Fe_2O_3 content for the $La_{1-x}FeO_{3-\delta}$ samples.

Fig. 8 reveals a perfect correlation between the hydrogen consumption determined for temperatures lower than 1073 K and the estimated amount of Fe_2O_3 (Table 4).

This result demonstrates that the low TPR temperature peaks can be assigned to the reduction of Fe_2O_3 clusters to Fe^0, thereby strongly supporting the hypothesis of the absence of cationic vacancies in $LaFeO_3$ perovskite when lanthanum content decreases. The reduction of the $LaFeO_3$ perovskite mainly occurs for temperatures higher than 1073 K but it cannot be excluded that the iron from the perovskite starts to reduce at lower temperatures. In the case of the LaFe sample (Table 4), the calculated reduction degree of Fe_2O_3 to Fe^0 (value higher than 100%), suggests that a small part of Fe^{3+} in the perovskite structure already starts to be reduced below 1073 K during the H_2-TPR experiment.

3.5. Total oxidation of methane

The activities of the $La_{1-x}FeO_{3-\delta}$ catalysts were evaluated in the CH_4 total oxidation reaction, which is a reaction largely used

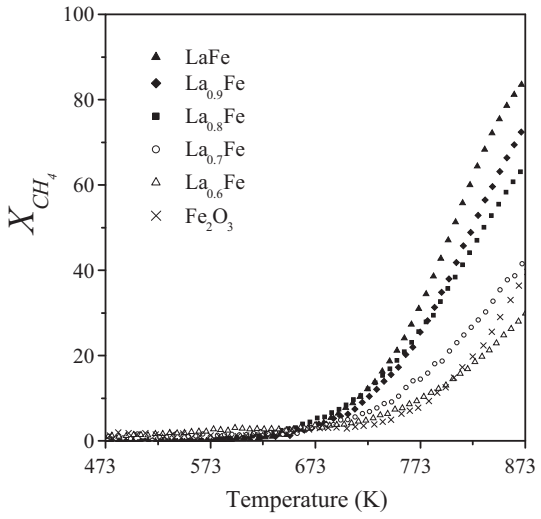

Fig. 9. Light-off curves for the total oxidation of methane in the presence of $La_{1-x}FeO_{3-\delta}$ mixed oxides.

for the determination of mixed-oxides reactivity [21,28,33,40,59]. Indeed, methane appears as a hydrocarbon particularly resistant to oxidation and a high temperature is required for its activation. Consequently, the reaction temperature is in the same range of order as that needed for the activation of the lattice oxygen of the catalysts. The obtained light-off curves are presented in Fig. 9.

As already reported by Ciambelli et al. over iron-based perovskite type oxides [40,63], CO_2 was the only oxidation product and no CO was detected during the total CH_4 oxidation reaction. Methane conversion started at about 623 K for all catalysts and an increase in the reaction temperature led to an increase in the CH_4 conversion with the observation of S-shaped oxidation curves. Big differences in catalytic activities were observed depending on the catalyst composition. For example, the temperature at 25% of CH_4 conversion increased with the decrease in lanthanum stoichiometry, from 758 K for LaFe to 853 K for $La_{0.6}Fe$. A similar trend was observed when comparing the CH_4 conversions obtained at 873 K with the same samples. Indeed, a CH_4 conversion of 85% was observed with the LaFe sample that exhibits the highest catalytic activity, while only 28% of methane was converted over the $La_{0.6}Fe$ sample.

The catalytic activity seemed to be directly linked to the solid stoichiometry, according to the following order: $LaFe > La_{0.9}Fe > La_{0.8}Fe > La_{0.7}Fe > La_{0.6}Fe$. Based on the structural, surface and redox properties of the $La_{1-x}FeO_{3-\delta}$ series, the catalytic activity was shown to decrease for increasing amount of surface Fe_2O_3. This trend is consistent with the proposed hypothesis concerning the distribution of iron in these mixed-oxides, namely a stoichiometric $LaFeO_3$ core onto which the excess of Fe is present as Fe_2O_3 clusters. The decrease in CH_4 total oxidation activity can then be ascribed to the decrease in the number of $LaFeO_3$-induced surface catalytic sites, related to the enrichment in Fe_2O_3 clusters on its surface and thus to the lower oxidation activity of Fe_2O_3 compared with that of $LaFeO_3$. In contrast with the results reported by Spinicci et al. [38], the catalytic activity decreased with the decrease in La content, indicating that our samples differ from the non-stoichiometric perovskites claimed by these authors and then strengthen our hypothesis of the existence of only stoichiometric oxides ($LaFeO_3$ and Fe_2O_3), irrespective of the lanthanum content in the mixed-oxide. This difference in the catalyst crystalline structure can easily be explained by the smoother synthesis conditions in the case of the solids prepared by Spinicci et al., especially due to the two steps procedure used by these authors to decompose the metal precursors. Such smoother conditions can therefore favor the formation of cationic vacancies in the perovskite network.

4. Conclusion

The main objective of this work was to study the influence of the $LaFeO_3$ perovskite stoichiometry on the catalytic activity in the total oxidation of methane. The various characterizations carried out over the $La_{1-x}FeO_{3-\delta}$ perovskite-type oxides prepared using the so-called self-combustion procedure allowed us to establish a correlation between the catalytic activity and the sample structure. The $LaFeO_3$ active sites composed of accessible oxygen on the surface associated to lattice iron and lanthanum cations, which usually behave as a reversible redox system, were progressively covered by Fe_2O_3 when decreasing the lanthanum stoichiometry of the solid. The presence of such surface iron oxide, as evidenced by XPS and XRD analyses, directly affected the catalytic system, which considerably hindered the access to the perovskite active sites. Based on all the characterization data, it was argued that this $La_{1-x}FeO_{3-\delta}$ series of samples prepared by the self-combustion method should only consist in stoichiometric oxides ($LaFeO_3$ and Fe_2O_3) whatever the lanthanum content in the mixed-oxide.

In summary, the total oxidation of methane over this series of $La_{1-x}FeO_{3-\delta}$ perovskites evidenced that the most efficient catalyst should present the stoichiometric $LaFeO_3$ composition and that the presence of an additional undesirable Fe_2O_3 crystalline phase on the surface is detrimental to catalytic activity.

References

[1] M.F.M. Zwinkels, S.G. Jaras, P.G. Menon, Catalysis Reviews: Science and Engineering 35 (1993) 319–358.
[2] P. Gelin, M. Primet, Applied Catalysis B 39 (2002) 1–37.
[3] T.V. Choudhary, S. Banerjee, V.R. Choudhary, Applied Catalysis A 234 (2002) 1–23.
[4] R. Prasad, L.A. Kennedy, E. Ruckenstein, Catalysis Reviews: Science and Engineering 26 (1984) 1–58.
[5] D. Ciuparu, E. Altman, L. Pfefferle, Journal of Catalysis 203 (2001) 64–74.
[6] K. Persson, A. Ersson, S. Colussi, A. Tovarelli, S.G. Jaras, Applied Catalysis B 66 (2006) 175–185.
[7] R. Strobel, S.E. Pratsinis, A.J. Baiker, Journal of Materials Chemistry 15 (2005) 605–610.
[8] A. Baylet, S. Royer, P. Marécot, J.M. Tatibouët, D. Duprez, Applied Catalysis B 77 (2008) 237–247.
[9] S. Ojala, N. Bion, A. Baylet, M. Tarighi, R.L. Keiki, D. Duprez, Applied Catalysis B 108-109 (2012) 22–31.
[10] D.B. Meadowcroft, Nature 226 (1970) 847–848.
[11] W.F. Libby, Science 171 (1971) 499–500.
[12] P.K. Gallagher, D.W. Johnson Jr., F. Schrey, Materials Research Bulletin 9 (1974) 1345–1352.
[13] T. Nitadori, M. Misono, Journal of Catalysis 93 (1985) 459–466.
[14] F. Souza Toniolo, R.N.S.H. Magalhães, C.A.C. Perez, M. Schmal, Applied Catalysis B 117–118 (2012) 156–166.
[15] L.G. Tejuca, J.L.G. Fierro, Properties and Application of Perovskite-Type Oxides, Dekker, New York, 1993.
[16] H. Arai, T. Yamada, K. Eguchi, T. Seiyama, Applied Catalysis 26 (1986) 265–276.
[17] H. Tanaka, I. Tan, M. Uenishi, N., Kajita, M., Taniguchi, Y., Sato, K., Narita, N., Sato, US Patent 7205257 (2005).
[18] G. Kremenic, K.M.G. Nieto, J.M.D. Tascon, L.G. Tejuca, Journal of the Chemical Society, Faraday Transactions 1 81 (1985) 939–949.
[19] T. Nitadori, T. Ichiki, M. Misono, Bulletin of the Chemical Society of Japan 61 (1988) 621–626.
[20] D.D. Agarwal, H.S. Goswami, Reaction Kinetics and Catalysis Letters 53 (1994) 441–449.
[21] A. Baiker, P.E. Marti, P. Keusch, E. Fritsch, A. Reller, Journal of Catalysis 146 (1994) 268–276.
[22] P.E. Marti, A. Baiker, Catalysis Letters 26 (1994) 71–84.
[23] H. Falcon, M.J. Martinez-Lope, J.A. Alonso, J.L.G. Fierro, Solid State Ionics 131 (2000) 237–248.
[24] R.J.H. Voorhoeve, J.P. Remeika Jr., L.E. Trimble, Annals of the New York Academy of Sciences 272 (1976) 3–21.
[25] S. Royer, D. Duprez, S. Kaliaguine, Journal of Catalysis 234 (2005) 364–375.
[26] T. Nakamura, M. Misono, Y. Yoneda, Bulletin of the Chemical Society of Japan 55 (1982) 394–399.
[27] D. Ferri, L. Forni, Applied Catalysis B 16 (1998) 119–126.
[28] S. Ponce, M.A. Pena, J.L.G. Fierro, Applied Catalysis B 24 (2000) 193–205.
[29] T. Nitadori, S. Kurihara, M. Misono, Journal of Catalysis 98 (1986) 221–228.

[30] R. Leanza, I. Rossetti, L. Fabbrini, C. Oliva, L. Forni, Applied Catalysis B 28 (2000) 55–64.
[31] Y. Zhang-Steenwinkel, J. Beckers, A. Bliek, Applied Catalysis A 235 (2002) 79–92.
[32] M. Alifanti, J. Kirchnerova, B. Delmon, Applied Catalysis A 245 (2003) 231–243.
[33] C. Batiot-Dupeyrat, F. Martinez-Ortega, M. Ganne, J.M. Tatibouet, Applied Catalysis A 206 (2001) 205–215.
[34] G. Sierra Gallego, F. Mondragon, J. Barrault, J.M. Tatibouet, C. Batiot-Dupeyrat, Applied Catalysis A 311 (2006) 164–171.
[35] G. Sierra Gallego, F. Mondragon, J. Barrault, J.M. Tatibouet, C. Batiot-Dupeyrat, Catalysis Today 133–135 (2008) 200–209.
[36] T. Roisnel, J. Rodriguez-Carvajal, Proceedings of the Seventh European Powder Diffraction Conference, 2000, pp. 118–123.
[37] A. Delmastro, D. Mazza, S. Ronchetti, M. Vallino, R. Spinicci, P. Brovetto, M. Salis, Materials Science and Engineering B 79 (2001) 140–145.
[38] R. Spinicci, A. Tofanari, A. Delmastro, D. Mazza, S. Ronchetti, Materials Chemistry and Physics 76 (2002) 20–25.
[39] G. Pecchi, P. Reyes, R. Zamora, L.E. Cadus, J.L.G. Fierro, Journal of Solid State Chemistry 181 (2008) 905–912.
[40] P. Ciambelli, S. Cimino, G. Lasorella, L. Lisi, S. De Rossi, M. Faticanti, G. Minelli, P. Porta, Applied Catalysis B 37 (2002) 231–241.
[41] Y. Wang, J. Zhu, L. Zhang, X. Yang, L. Lu, X. Wang, Materials Letters 60 (2006) 1767–1770.
[42] D. Berger, C. Matei, F. Papa, G. Voicu, V. Fruth, Progress in Solid State Chemistry 35 (2007) 183–191.
[43] C. Batiot-Dupeyrat, G. Valderrama, A. Meneses, F. Martinez, J. Barrault, J.M. Tatibouet, Applied Catalysis A 248 (2003) 143–151.
[44] F. Martinez-Ortega, C. Batiot-Dupeyrat, G. Valderrama, J.M. Tatibouet, Comptes Rendus de l'Academie des Sciences, Serie IIc: Chimie 4 (2001) 49–55.
[45] A. Civera, M. Pavese, G. Saracco, V. Specchia, Catalysis Today 83 (2003) 199–211.
[46] Z.Q. Tian, H.T. Yu, Z.L. Wang, Materials Chemistry and Physics 106 (2007) 126–129.
[47] H.P. Kumar, C. Yijayakumar, C.N. George, S. Solomon, R. Jose, J.K. Thomas, J. Koshy, Journal of Alloys and Compounds 458 (2008) 528–531.
[48] S. Royer, F. Bérubé, S. Kaliaguine, Applied Catalysis A 282 (2005) 273–284.
[49] G. Shabbir, A.H. Qureshi, K. Saeed, Materials Letters 60 (2006) 3706–3709.
[50] B.P. Barbero, J.A. Gamboa, L.E. Cadús, Applied Catalysis B 65 (2006) 21–30.
[51] L. Xi, L. Xiaoxun, X. Baokun, Z. Muyu, Journal of Alloys and Compounds 186 (1992) 315–319.
[52] X. Li, H. Zhang, X. Liu, S. Li, M. Zhao, Materials Chemistry and Physics 38 (1994) 355–362.
[53] H. Taguchi, A. Sugita, M. Nagao, Journal of Solid State Chemistry 119 (1995) 164–168.
[54] J.L.G. Fierro, L.G. Tejuca, Applied Surface Science 27 (1987) 453–457.
[55] N.S. McIntyre, D.G. Zetaruk, Analytical Chemistry 49 (1977) 1521–1529.
[56] M.P. Rosynek, D.T. Magnuson, Journal of Catalysis 48 (1977) 417–421.
[57] Y.U. Teterin, A.Y. Teterin, A.M. Lebedev, K.E. Ivanov, Journal of Electron Spectroscopy and Related Phenomena 137–140 (2004) 607–612.
[58] D.D. Hawn, B.M. DeKoven, Surface and Interface Analysis 10 (1987) 63–74.
[59] S. Petrović, A. Terlecki-Baričević, Lj Karanović, P. Kirilov-Stefanov, M. Zdujić, V. Dondur, D. Paneva, I. Mitov, V. Rakić, Applied Catalysis B 79 (2008) 186–198.
[60] G. Munteanu, L. Ilieva, D. Andreeva, Thermochimica Acta 291 (1997) 171–177.
[61] H.Y. Lin, Y.W. Chen, C. Li, Thermochimica Acta 400 (2003) 61–67.
[62] O.J. Wimmers, P. Arnoldy, J.A. Moulijn, Journal of Physical Chemistry 90 (1986) 1331–1337.
[63] P. Ciambelli, S. Cimino, L. Lisi, M. Faticanti, G. Minelli, I. Pettiti, P. Porta, Applied Catalysis B 33 (2001) 193–203.